Proceedings of the 9th International and 49th National Conference on Fluid Mechanics and Fluid Power (FMFP)
December 14-16, 2022, IIT Roorkee, Roorkee-247667, Uttarakhand, India

FMFP2022-12-2022

Fluid-Structure Interaction with an Updated Lagrangian Smoothed Particle Hydrodynamics

Dinesh Adepu[1], Prabhu Ramachandran[1]

[1]Department of Aerospace Engineering, Indian Institute of Technology Bombay, Powai, Mumbai 400076, India

ABSTRACT A corrected transport velocity formulation (CTVF) based solver is developed to study the deformation of elastic structures under hydrodynamic loads. CTVF is adopted to handle both fluid and structural dynamics. The current solver's advantage is to eliminate inhomogeneous particle distribution in fluid flow and tensile instability in elastic structures. A ghost particle-based approach is used to handle the coupling between the fluid and solid phases. The proposed scheme is verified by simulating a few test cases, which we validate with exact analytical solutions. As an application, we simulate an elastic plate deformation due to dam-breaking fluid.

Keywords: Smoothed particle hydrodynamics; Fluid-structure interaction; Transport velocity formulation

I. INTRODUCTION

Fluid-structure interaction (FSI) is a common engineering problem that is seen in daily life. Some examples include the deformation of the wind turbine blade due to the fluid flow, the flow traversal due to the deflected blade, blood flow in heart value, coastal engineering, and vortex-induced vibration [28], [5]. An accurate study of FSI can allow us to optimize the systems where FSI is dominant. However, studying the FSI phenomena through experiments or analytical techniques is complex due to its nonlinear behavior.

Mesh-based schemes such as finite element method (FEM) [14] and finite volume method (FVM) [11] have been used for the last few decades in modeling the FSI problems. However, mesh-based methods are not favorable when dealing with free surface flow problems or problems involving large deformation of the structure. This is due to explicit free surface tracking, and mesh distortion [16] while dealing with large deformation solids. Therefore, meshless methods are preferred while handling FSI problems involving free surfaces, multiphase flows, and large deformation in solids. The smoothed particle hydrodynamics (SPH) and material point method (MPM) are more commonly used to model the fluid phase. While the solids are modeled with SPH or Reproducing Kernel Particle Methods (RKPM), or the Discrete Element Method (DEM) [9], [13]. These meshless techniques have been coupled for the past two decades to model the fluid-structure interaction. A few schemes with SPH and MPM are SPH-DEM [29], SPH-TLSPH [22], SPH-RKPM [19], SPH-Peridynamics [26], MPM-DEM [23]. For more, see the review by [12]. In the current work, we use SPH to handle FSI problems.

In SPH, fluids are modeled primarily using two approaches, one by assuming they are weakly compressible and another by considering them incompressible. Though SPH is successful in modeling fluid flows, it suffers from particle pairing and irregular particle distribution problems resulting in poor function approximation [21] and unstable simulations. To homogenize the particles, [30] adjusts the particle positions after each timestep. Then, the particle properties are adjusted to the new position using Taylor series approximation. Later, Adami [2] proposed a transport velocity formulation (TVF) scheme where the particles are moved with a "transport velocity" rather than the momentum velocity. TVF is applied to internal fluid flow problems. Zhang [32] extended the TVF formulation and called it the generalized TVF (GTVF) and applied it to free surface problems and elastic solids. However, while extending TVF, GTVF has missing terms and is sensitive to the particle shifting technique (PST). [3] proposed a corrected TVF (CTVF) scheme where the missing terms in TVF are incorporated and is robust to the PST. While handling elastic solids with SPH, the classical SPH [8] faces tensile instability and results in numerical fracture. [8] has proposed adding artificial stress, [7] introduces stress-points in addition to the existing particles, [24] modifies the equation of state to eliminate the tensile instability. CTVF can eliminate tensile instability and handle higher Poisson ratios. While CTVF is also robust to different PST. FSI in SPH is modeled by several works, such as, WCSPH-Total Lagrangian SPH (TLSPH) [31], WCSPH-Updated Lagrangian SPH (ULSPH) [4], ISPH-TLSPH[22].

Handling FSI problems with the transport velocity formulation framework is advantageous as it can solve the tensile instability issue in solid dynamics and inhomogeneous particle distribution in fluids. In the current work, we handle FSI problems by the CTVF method, where both fluids and solid phases are modeled using CTVF alone. To validate the proposed method, we consider three numerical test cases. A uniformly distributed load over a clamped beam (UDL) problem is considered to validate the elastic dynamics of CTVF. An aluminum plate over a hydrostatic tank for FSI validation is considered. Finally, it is applied to a fluid flow hitting an elastic plate. Here, the deformation of the elastic plate is compared against the experimental results. A convergence analysis is undertaken for both UDL and elastic deformation under hydrodynamic load problems.

II. METHODOLOGY

We follow CTVF formulation to model the fluid and solid phase. Following CTVF, the particles are moved with a transport velocity rather than the momentum velocity, with which we get a homogenized particle distribution as well as it eliminates the tensile instability. In the next two sections we show the discretized equations of both fluid and solid phase. Please see [3] for more details.

A. Discrete equations of the fluid medium

The governing equations of the fluid are conservation of mass and momentum. Following the weakly compressible SPH

scheme, we use an equation of state to complete the system. The SPH discretization of the continuity equation (1) and the EDAC based [20] pressure evolution equation (2) respectively are,

$$\frac{\tilde{d}\rho_a}{dt} = \sum_b \frac{m_b}{\rho_b} \left(\rho_a \, \tilde{\mathbf{u}}_{ab} + (\rho \, (\tilde{\mathbf{u}} - \mathbf{u}))_{ab}\right) \cdot \nabla_a W_{ab}, \quad (1)$$

$$\frac{\tilde{d}p_a}{dt} = \sum_b \frac{m_b}{\rho_b} \Bigg((p_a - \rho_a c_s^2) \, \mathbf{u}_{ab} + p_a \, \tilde{\mathbf{u}}_{ab} - (p \, (\tilde{\mathbf{u}} - \mathbf{u}))_{ab} + 4 \, \nu_{edac} \frac{p_a - p_b}{(\rho_a + \rho_b)(r_{ab}^2 + 0.01 h_{ab}^2)} \mathbf{r}_{ab} \Bigg) \cdot \nabla_a W_{ab}. \quad (2)$$

Where $\frac{\tilde{d}}{dt}$ is the material derivative, with $\tilde{u}$ being the transport velocity of the particles, $\mathbf{u}_{ab} = \mathbf{u}_a - \mathbf{u}_b$. Similarly, the discretized momentum equation for fluids is written as,

$$\frac{\tilde{d}\mathbf{u}_a}{dt} = -\sum_b m_b \left[\left(\frac{p_a}{\rho_a^2} + \frac{p_b}{\rho_b^2} \right) \mathbf{I} - \left(\frac{\mathbf{A}_a}{\rho_a^2} + \frac{\mathbf{A}_b}{\rho_b^2} + \Pi_{ab} \mathbf{I} \right) \right] \cdot \nabla_a W_{ab} + \mathbf{u}_a \sum_b \frac{m_b}{\rho_b} \, \tilde{\mathbf{u}}_{ab} \cdot \nabla_a W_{ab} + \sum_b m_b \frac{4\eta \nabla W_{ab} \cdot \mathbf{r}_{ab}}{(\rho_a + \rho_b)(r_{ab}^2 + 0.01 h_{ab}^2)} \mathbf{u}_{ab} + \mathbf{g}_a + \frac{\mathbf{F}_{\text{FSI}}^a}{m_a} \quad (3)$$

where $\mathbf{A}_a = \rho_a \mathbf{u}_a \otimes (\tilde{\mathbf{u}}_a - \mathbf{u}_a)$, $\mathbf{I}$ is the identity matrix, η is the kinematic viscosity of the fluid and [17] formulation is used to discretize the viscosity term. Π_{ab} is the artificial viscosity [15] to maintain the stability of the numerical scheme. It is given as,

$$\Pi_{ab} = \begin{cases} \frac{-\alpha h_{ab} \bar{c}_{ab} \phi_{ab}}{\bar{\rho}_{ab}} & \mathbf{u}_{ab} \cdot \mathbf{r}_{ab} < 0, \\ 0 & \mathbf{u}_{ab} \cdot \mathbf{r}_{ab} \geq 0, \end{cases} \quad (4)$$

where,

$$\phi_{ab} = \frac{\mathbf{u}_{ab} \cdot \mathbf{r}_{ab}}{r_{ab}^2 + 0.01 h_{ab}^2}, \quad (5)$$

where, $\mathbf{r}_{ab} = \mathbf{r}_a - \mathbf{r}_b$, $h_{ab} = (h_a + h_b)/2$, $\bar{\rho}_{ab} = (\rho_a + \rho_b)/2$, $\bar{c}_{ab} = (c_a + c_b)/2$, and α is the artificial viscosity parameter. $\mathbf{F}_{\text{FSI}}^a$ is the force due to the interaction with elastic structure. This force modeling is explained in section II-D. We utilize the ghost particle approach proposed in [1] to handle the boundaries.

B. Solid phase modeling

Similar to discretized fluid governing equation, the elastic structure equations are (1), and the momentum equation,

$$\frac{\tilde{d}\mathbf{u}_a}{dt} = -\sum_b m_b \left[\left(\frac{p_a}{\rho_a^2} + \frac{p_b}{\rho_b^2} \right) \mathbf{I} - \left(\frac{\boldsymbol{\sigma}_a^{'}}{\rho_a^2} + \frac{\boldsymbol{\sigma}_b^{'}}{\rho_b^2} + \Pi_{ab} \mathbf{I} \right) \right] \cdot \nabla_a W_{ab} + \mathbf{g}_a + \frac{\mathbf{F}_{\text{FSI}}^a}{m_a}, \quad (6)$$

while the additional stress terms, $\mathbf{A}$ in momentum equation of solid mechanics are not considered as it has a negligible effect. An equation of state is utilized to link the pressure with density following a weakly compressible SPH scheme. Jaumann stress rate equation is solved to evolve the shear stress, given as,

$$\frac{\tilde{d}\boldsymbol{\sigma}_a^{'}}{dt} = 2G(\dot{\boldsymbol{\epsilon}}_a - \frac{1}{3}\dot{\boldsymbol{\epsilon}}_a \mathbf{I}) + \boldsymbol{\sigma}_a^{'} \boldsymbol{\Omega}_a^T + \boldsymbol{\Omega}_a \boldsymbol{\sigma}_a^{'} \quad (7)$$

The SPH discretization of the gradient of velocity is given as,

$$\nabla \mathbf{u}_a = -\sum_b \frac{m_b}{\rho_b} (\mathbf{u}_a - \mathbf{u}_b) \otimes (\nabla_a W_{ab}), \quad (8)$$

where $\otimes$ is the outer product. With the strain and rotation tensors as,

$$\dot{\epsilon}_{ij} = \frac{1}{2} \left(\frac{\partial u_i}{\partial x_j} + \frac{\partial u_j}{\partial x_i} \right), \quad (9)$$

and Ω_{ij} is the rotation tensor,

$$\Omega_{ij} = \frac{1}{2} \left(\frac{\partial u_i}{\partial x_j} - \frac{\partial u_j}{\partial x_i} \right). \quad (10)$$

C. Transport velocity computation

The particles in the current scheme are moved with the transport velocity,

$$\frac{d\mathbf{r}_a}{dt} = \tilde{\mathbf{u}}_a. \quad (11)$$

The transport velocity is updated using,

$$\tilde{\mathbf{u}}_a(t + \Delta t) = \mathbf{u}_a(t) + \Delta t \, \frac{\tilde{d}\mathbf{u}_a}{dt} + \left(\frac{d\mathbf{u}_a}{dt} \right)_{\text{c}} \Delta t \quad (12)$$

Where $\left(\frac{d\mathbf{u}_a}{dt}\right)_{\text{c}}$ is the homogenization acceleration which ensures that the particle positions are homogeneous. In the current work we have used Sun's [25] PST to homogenization the fluid medium while iterative PST (IPST)[10] for the solid phase. According to [3] the force formulation of [25] is,

$$\left(\frac{d\mathbf{u}_a}{dt} \right)_{\text{c}} = -\frac{\text{M} \, (2h) c_0}{\Delta t} \sum_b \left[1 + R \left(\frac{W_{ab}}{W(\Delta x)} \right)^n \right] \nabla_a W_{ab} V_b, \quad (13)$$

where R is an adjustment factor to handle the tensile instability, and M is the mach number of the flow. V_b is the volume of the b^{th} particle, c_0 is the speed of sound. The acceleration is modified to account for particles on the free surface. Here, $R = 0.2$ and $n = 4$ are used. Please see [3] for detailed explanation of PST.

D. Fluid-structure interaction

Coupling is handled in a straight forward way in SPH. While modelling the fluid phase and treating the fluid-structure interactions, the structure particles are assumed to be boundary particles. From the boundary handling given in Adami [1], we compute the pressure of the boundary particles from the extrapolated equation as,

$$p_s = \frac{\Sigma_f p_f W_{sf} + (\mathbf{g} - \mathbf{a}_\mathbf{s}) \cdot \Sigma_f \rho_f \mathbf{r}_{sf} W_{sf}}{\Sigma_f W_{sf}}. \quad (14)$$

Here, $\mathbf{a}_s$ is the acceleration of the structure particles. The subscript f denotes the fluid particles and s denotes the structure particles. By the extrapolated pressure, hydrodynamic density of structure properties are computed. Please note that the pressure we set here are only pertaining to the FSI force and does not correspond to the real pressure or density of the structure particles. By utilizing the previously set hydrodynamic properties on the structure, the interaction force is computed using,

$$\mathbf{F}_{\text{FSI}}^i = -m_i \sum_a m_a \left(\frac{p_i}{\rho_i^2} + \frac{p_a}{\rho_a^2} + \Pi_{ia} \right) \nabla_i W(x_{ia}) \quad (15)$$

where i is fluid particle, a is structure particle.

III. RESULTS AND DISCUSSION

A. Uniformly distributed loading (UDL) on a clamped beam

In the first test case, we validate the structural part of the current solver. We chose a homogeneous elastic plate clamped on both ends acted upon by a uniformly distributed load ($q = 20$ Nm^{-1}) as shown in fig. 1. The beam's length (L) and height (H) is 0.2 m and 0.012 m, respectively. The mechanical properties

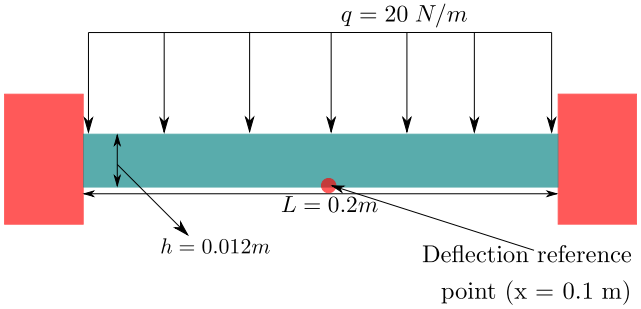

Figure 1: **The schematic of a clamped elastic beam being acted upon by a uniformly distributed load.**

of the plate are set as $E = 10^7$ Pa in Young's modulus, $\nu = 0$ in Poisson's ratio and $\rho = 1000$ kgm^{-3}) in density. The numerical solution of the y-displacement at the center of the beam is compared against the analytical counterpart. The analytical solution for the deflection of a uniformly distributed beam clamped at both ends is given by

$$\eta\left(\frac{L}{2}\right) = \frac{qL^4}{384D}, \tag{16}$$

where, D is defined as $\frac{Eh^3}{12(1-(\nu)^2)}$. We consider three particle resolutions such that, 10, 15, and 20 particles along the beam's width are used. We run for a total physical time of 2 seconds.

Figure 2 depicts the time history of y-displacement of the beam center for different particle resolutions computed using the current solver compared against the analytical solution. From fig. 2, we can see that the current solver can accurately predict the displacement of the clamped beam. Convergence of the current scheme is captured in fig. 2, and the computational results are within a reasonable variation of the analytical solution with the variation of the particle spacing.

B. Hydrostatic water column on an elastic plate

In this example we study the deformation of an elastic plate due to the hydrostatic water column. We utilise the current example to examine the accuracy and convergence of the current solver. The schematic of fluid with the elastic beam is shown in fig. 3 along with the initial pressure distribution in the fluid. The figure includes the dimensions as well. The material properties of the beam are, a density of 2700 kgm^{-3}, with an Young's modulus of 67.5 GPa, and a Poisson ratio of 0.34. The material properties of the fluid are, a density of 1000 kgm^{-3}, with a dynamic viscosity of 0 kgm^{-1}s^{-1}. We consider two particle resolutions such that we get 10, 15 and 20 particles along the width directing of the beam. We run the simulation for a total physical time of 3 seconds. The y-displacement at the center of the beam is compared against the analytical with the current numerical solver for quantitative validation. Here, the beam deflection computed using an analytical expression results in a deflection $d = -6.85 \times 10^{-5}$ m.

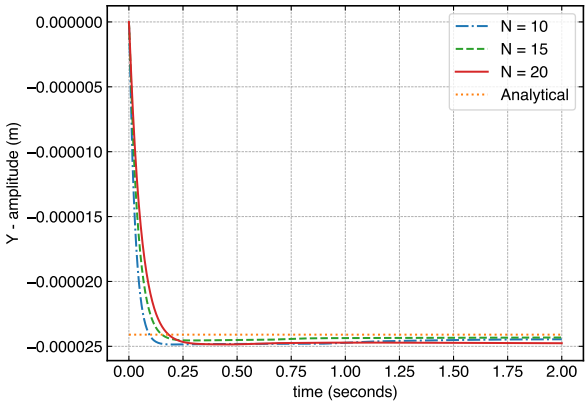

Figure 2: **Time variation of the y-displacement of the center of the beam for three different resolutions, compared against the analytical result.**

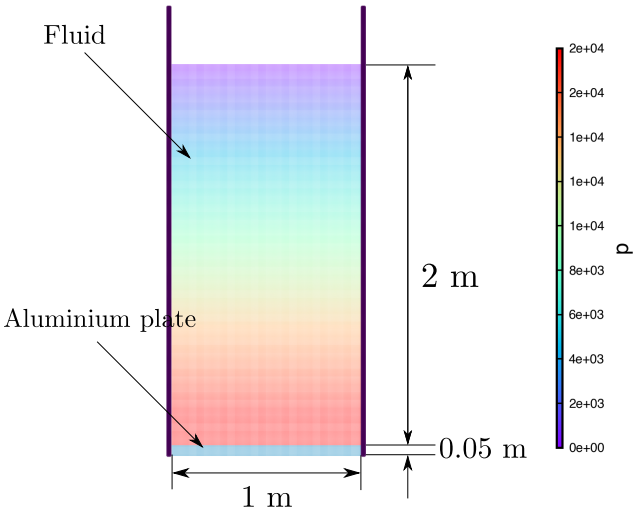

Figure 3: **Schematic of the hydrostatic water column on an elastic plate. Fluid particle color represents pressure.**

Figure 4 shows the particle plot of the fluid along with the elastic solid at time 2 seconds with color of the fluid particles describing the pressure. This snapshot corresponds to the highest particle resolution i.e., 20 particles along the width direction. From the fig. 4, we can see that the current solver produces a smooth pressure distribution demonstrating the stability of the current solver. Figure 5 depicts the time history of y-displacement of the beam center for different particle resolutions computed using the current solver compared against the analytical solution. From fig. 5 we can see that the current solver is able to predict the displacement of the clamped beam within the vicinity of the analytical results. Also as the particle spacing is reduced, the beam displacement is converging as well.

C. Water impact onto an elastic plate

In this case, we study the deformation of the elastic plate due to the impact of a dam breaking flow. Figure 6 shows the initial positions of fluid and the structure inside the dam, including the dimensions. Following [27] we set the material

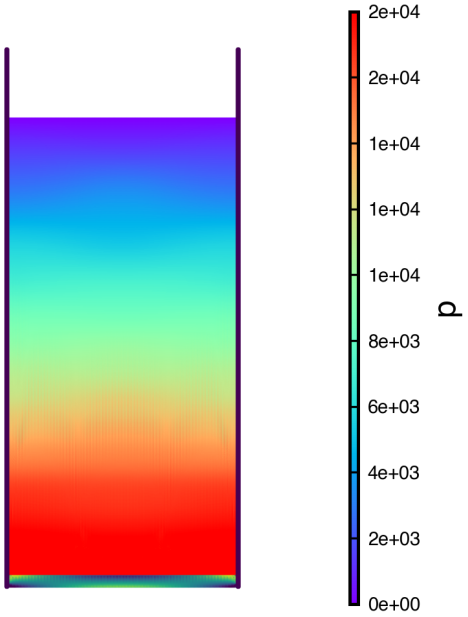

Figure 4: **Snapshot of the fluid and the elastic structure at time 0.5 sec including the pressure of the fluid.**

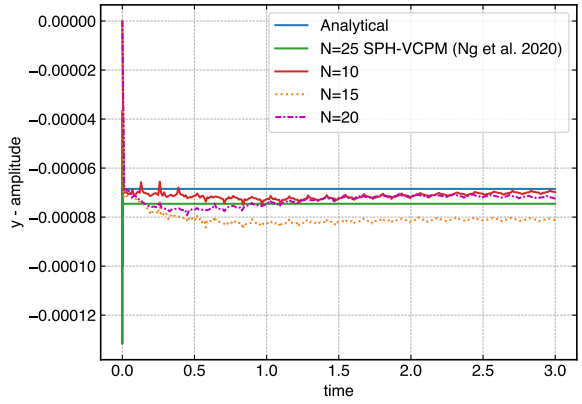

Figure 5: **The mid-span deflection of the structure under hydrodynamic loading with time for different resolutions, compared against the analytical and the numerical result of [18]**

properties of the elastic plate, a density of 2500 kgm^{-3}, with an Young's modulus of 10^6 Pa, and a Poisson ratio of 0. The material properties of the fluid are, a density of 1000 kgm^{-3}, with a dynamic viscosity of 0 kgm^{-1}s^{-1}. A particle spacing of 5×10^{-4} m is taken, resulting in a total of 182911 particles, which includes fluid, structure and solid wall. We run a total physical time of 0.7 seconds. Here the fluid is initially released which attains a certain velocity by the time it impacts the structure. The structure will obstruct the fluid making it rise and the fluid will deform the elastic plate. The fluid will rise and hit the other end of the dam, following it comes back and hits the structure from the back. For a quantitative validation, we compare the current solver results to the other numerical techniques.

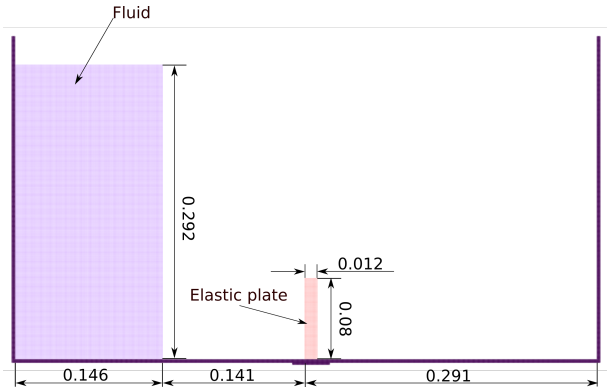

Figure 6: **Schematic of the dam-break flow impacting an elastic plate. All dimensions are in meters.**

Figure 7 shows the snapshots of the fluid and the elastic structure at different time instances. From fig. 7, we can see that the fluid after hitting the structure rises and hits the other end of the tank and travels back to hit the structure again. The time variation of the x-displacement of the elastic structure is compared against other numerical results [27], [6]. From the fig. 8 we can see that the displacement computed by the current solver is with in a vicinity of the other results produced.

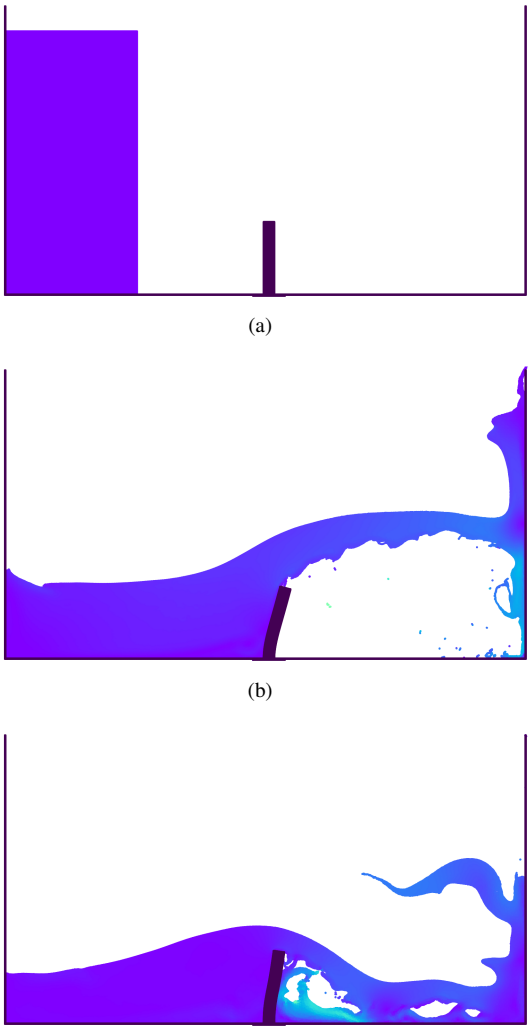

Figure 7: **(a) Snapshot of the fluid and the structure at different time stamps - Water impact onto an elastic plate.**

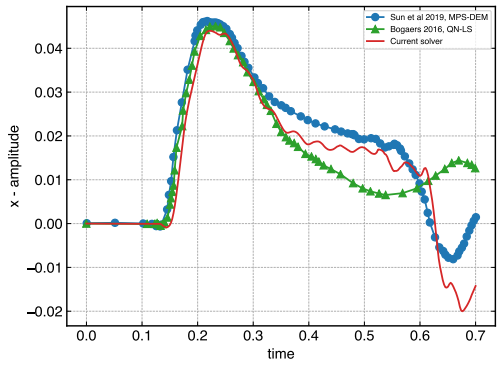

Figure 8: **Time histories of horizontal displacement of the free end of the elastic structure compared against the numerical results of [27], [6]- Water impact onto an elastic plate.**

IV. CONCLUSIONS

CTVF is able eliminate several issues SPH faces while solving fluid and solid problems. Through particle shifting techniques as well as incorporating the missing terms CTVF is able to produce better approxmiation in simulating fluid problmes, also it is adaptable to different PST techniqes. Similarly with PST the newly CTVF eliminates tensile instability while solving the elastic dynamics probnlems. With the adavantages in mind, we solve both fluid and solid phases in simulating FSI problems with CTVF with this approach we are able to handle FSI problems.

We validated the current schemes by solving a UDL problem to test the structure equations and an aluminium plate over a hydrostatic tank where an analytical solution is available is utilized to validate the FSI part of the current solver. The current solver is applied to wave front arising due to a dam break hitting a steady elastic plate, here the deformation of the elastic plate is compared against the experimental results. A convergence analysis is undertaken for both fundamental benchmarks, UDL and hydrostatic tank.

For the future work, we plan to extend the current solver being extended to handle the anisotropic structures and 3D FSI problems.

REFERENCES

[1] S. Adami, X.Y. Hu, and N.A. Adams, *A generalized wall boundary condition for smoothed particle hydrodynamics*, Journal of Computational Physics **231** (2012), no. 21, 7057–7075.

[2] Stefan Adami, XY Hu, and Nikolaus A Adams, *A transport-velocity formulation for smoothed particle hydrodynamics*, Journal of Computational Physics **241** (2013), 292–307.

[3] Dinesh Adepu and Prabhu Ramachandran, *A corrected transport-velocity formulation for fluid and structural mechanics with sph*, arXiv preprint arXiv:2106.00756 (2021).

[4] Carla Antoci, Mario Gallati, and Stefano Sibilla, *Numerical simulation of fluid–structure interaction by sph*, Computers & structures **85** (2007), no. 11-14, 879–890.

[5] PW Bearman, *Circular cylinder wakes and vortex-induced vibrations*, Journal of Fluids and Structures **27** (2011), no. 5-6, 648–658.

[6] Alfred EJ Bogaers, Schalk Kok, B Dayanand Reddy, and Thierry Franz, *An evaluation of quasi-newton methods for application to fsi problems involving free surface flow and solid body contact*, Computers & Structures **173** (2016), 71–83.

[7] CM Chalk, M Pastor, J Peakall, DJ Borman, PA Sleigh, W Murphy, and R Fuentes, *Stress-particle smoothed particle hydrodynamics: An application to the failure and post-failure behaviour of slopes*, Computer Methods in Applied Mechanics and Engineering **366** (2020), 113034.

[8] James P Gray, Joseph J Monaghan, and RP1021 Swift, *Sph elastic dynamics*, Computer methods in applied mechanics and engineering **190** (2001), no. 49-50, 6641–6662.

[9] Patrick Hu, Liping Xue, Shaolin Mao, Ramji Kamakoti, Hongwu Zhao, Nagendra Dittakavi, Kan Ni, Zhen Wang, and Qingding Li, *Material point method applied to fluid-structure interaction (fsi)/aeroelasticity problems*, 48th AIAA aerospace sciences meeting including the new horizons forum and aerospace exposition, 2010, p. 1464.

[10] C. Huang, T. Long, S.M. Li, and M.B. Liu, *A kernel gradient-free SPH method with iterative particle shifting technology for modeling low-Reynolds flows around airfoils*, Engineering Analysis with Boundary Elements **106** (2019), 571–587 (en).

[11] Hrvoje Jasak, *Updated lagrangian finite volume solver for large deformation dynamic response of elastic body*, Transactions of FAMENA **31** (2007), no. 1, 55.

[12] Abbas Khayyer, Hitoshi Gotoh, and Yuma Shimizu, *On systematic development of fsi solvers in the context of particle methods*, Journal of Hydrodynamics **34** (2022), no. 3, 395–407.

[13] Xinpo Li, Jun Yao, Yulian Sun, and Yong Wu, *Material point method analysis of fluid–structure interaction in geohazards*, Natural Hazards (2022), 1–19.

[14] Alexander Lozovskiy, Maxim A Olshanskii, Victoria Salamatova, and Yuri V Vassilevski, *An unconditionally stable semi-implicit fsi finite element method*, Computer Methods in Applied Mechanics and Engineering **297** (2015), 437–454.

[15] J. J. Monaghan, *Smoothed Particle Hydrodynamics*, Reports on Progress in Physics **68** (2005), 1703–1759.

[16] Louis Moresi, Frédéric Dufour, and H-B Mühlhaus, *A lagrangian integration point finite element method for large deformation modeling of viscoelastic geomaterials*, Journal of computational physics **184** (2003), no. 2, 476–497.

[17] Joseph P. Morris, Patrick J. Fox, and Yi Zhu, *Modeling low reynolds number incompressible flows using SPH*, Journal of Computational Physics **136** (1997), no. 1, 214–226.

[18] KC Ng, A Alexiadis, Hailong Chen, and TWH Sheu, *A coupled smoothed particle hydrodynamics-volume compensated particle method (sph-vcpm) for fluid structure interaction (fsi) modelling*, Ocean Engineering **218** (2020), 107923.

[19] Yu-Xiang Peng, A-Man Zhang, and Shi-Ping Wang, *Coupling of wcsph and rkpm for the simulation of incompressible fluid–structure interactions*, Journal of Fluids and Structures **102** (2021), 103254.

[20] Prabhu Ramachandran and Kunal Puri, *Entropically damped artificial compressibility for SPH*, Proceedings of the 6th International Conference on Computational Methods 5 conference (Auckland, New Zealand) (G. R. Liu and Raj Das, eds.), vol. 2, 14th – 17th, July 2015, p. Paper ID 1210.

[21] P Rastelli, R Vacondio, JC Marongiu, G Fourtakas, and Benedict D Rogers, *Implicit iterative particle shifting for meshless numerical schemes using kernel basis functions*, Computer Methods in Applied Mechanics and Engineering **393** (2022), 114716.

[22] AM Salehizadeh and AR Shafiei, *A coupled isph-tlsph method for simulating fluid-elastic structure interaction problems*, Journal of Marine Science and Application **21** (2022), no. 1, 15–36.

[23] Veronika Singer, Klaus B Sautter, Antonia Larese, Roland Wüchner, and Kai-Uwe Bletzinger, *A partitioned material point method and discrete element method coupling scheme*, Advanced Modeling and Simulation in Engineering Sciences **9** (2022), no. 1, 1–24.

[24] Keisuke Sugiura and Shu-ichiro Inutsuka, *An extension of godunov sph ii: Application to elastic dynamics*, Journal of Computational Physics **333** (2017), 78–103.

[25] P.N. Sun, A. Colagrossi, S. Marrone, M. Antuono, and A.-M. Zhang, *A consistent approach to particle shifting in the delta - Plus -SPH model*, Computer Methods in Applied Mechanics and Engineering **348** (2019), 912–934 (en).

[26] Wei-Kang Sun, Lu-Wen Zhang, and KM Liew, *A smoothed particle hydrodynamics–peridynamics coupling strategy for modeling fluid–structure interaction problems*, Computer Methods in Applied Mechanics and Engineering **371** (2020), 113298.

[27] Yijie Sun, Guang Xi, and Zhongguo Sun, *A fully lagrangian method for fluid–structure interaction problems with deformable floating structure*, Journal of Fluids and Structures **90** (2019), 379–395.

[28] Charles HK Williamson, R Govardhan, et al., *Vortex-induced vibrations*, Annual review of fluid mechanics **36** (2004), no. 1, 413–455.

[29] Ke Wu, Dongmin Yang, and Nigel Wright, *A coupled sph-dem model for fluid-structure interaction problems with free-surface flow and structural failure*, Computers & Structures **177** (2016), 141–161.

[30] Rui Xu, Peter Stansby, and Dominique Laurence, *Accuracy and stability in incompressible sph (isph) based on the projection method and a new approach*, Journal of computational Physics **228** (2009), no. 18, 6703–6725.

[31] Ling Zhan, Chong Peng, Bingyin Zhang, and Wei Wu, *A stabilized tl–wc sph approach with gpu acceleration for three-dimensional fluid–structure interaction*, Journal of Fluids and Structures **86** (2019), 329–353.

[32] Chi Zhang, Xiangyu Y Hu, and Nikolaus A Adams, *A generalized transport-velocity formulation for smoothed particle hydrodynamics*, Journal of Computational Physics **337** (2017), 216–232.